Numerical Benchmark of Turbulence modelling in Gas Turbine Rotor-Stator System

Riccardo da Soghe, Luca Innocenti, Antonio Andreini, Sébastien Poncet

Proceedings of ASME TURBO EXPO 2010: Power for Land, Sea & Air
GT2010
June 14-18, 2010, Glasgow, GB

GT2010-22627

DRAFT
NUMERICAL BENCHMARK OF TURBULENCE MODELING IN GAS TURBINE ROTOR-STATOR SYSTEM

Riccardo Da Soghe, Luca Innocenti, Antonio Andreini
Energy Engineering Department "S.Stecco"
University of Florence
50139, via S.Marta 3, Florence, Italy
Tel: (+39)0554796618, Fax: (+39)0554796342
Email: riccardo.dasoghe@htc.de.unifi.it

Sébastien Poncet
Laboratoire M2P2, Technopôle Château-Gombert
38 rue F. Joliot-Curie, 13451 Marseille, France
Tel: (+33) (0)4 91 11 85 23
Fax: (+33) (0)4 91 11 85 02
Email: poncet@L3m.univ-mrs.fr

ABSTRACT

Accurate design of the secondary air system is one of the main tasks for reliability and performance of gas turbine engines. The selection of a suitable turbulence model for the study of rotor-stator cavity flows, which remains an open issue in the literature, is here addressed over a wide range of operating conditions. A numerical benchmark of turbulence models is indeed proposed in the case of rotor-stator disk flows with and without superimposed throughflow.

The predictions obtained by the means of several two equation turbulence models available within the CFD solver Ansys CFX 12.0 are compared with those previously evaluated by Poncet et *al*. (1; 2) through the Reynolds Stress Model (RSM) of Elena and Schiestel (3; 4) implemented in a proprietary finite volume code. The standard k-ε and k-ω SST models including high and low Reynolds approaches, have been used for all calculations presented here. Further more, some tests were conduced using the innovative k-ω SST-CC and k-ω SST-RM models that take into account the curvature effects via the Spalart-Shur correction term (5) and the reattachement modification proposed by Menter (6) respectively. The numerical calculations have been compared to extensive velocity and pressure measurements performed on the test rig of the IRPHE's laboratory in Marseilles (1; 2).

Several configurations, covering a wide range of real engine operating conditions, were considered. The influence of the typical non dimensional flow parameters (Reynolds number and flowrate coefficient) on the flow structure is studied in detail. In the case of an enclosed cavity, the flow exhibits a Batchelor-like structure with two turbulent boundary layers separated by a laminar rotating core. When an inward axial throughflow is superimposed, the flow remains of Batchelor type with a core rotating faster than the disk because of conservation of the angular momentum. In this case, turbulence intensities are mainly confined close to the stator. Turbulence models based on a low Reynolds approach provide better overall results for the mean and turbulent fields especially within the very thin boundary layers. The standard k-ω SST model offers the best trade-off between accuracy and computational cost for the parameters considered here. In the case of an outward throughflow, the k-ω SST in conjunction with a low Reynolds approach and RSM models provide similar results and predict quite well the transition from the Batchelor to the Stewartson structures.

NOMENCLATURE

a	Radius of the hub	$[m]$
b	Outer radius of the rotating disk	$[m]$
h	Interdisk spacing	$[m]$
j_h	Radial gap between the hub and the stator	$[m]$
j_s	Radial gap between the rotor and the shroud	$[m]$
k	Turbulence kinetic energy	$[m^2/s^2]$
P	Pressure	$[Pa]$
Q	Voluminal flowrate	$[m^3/s]$
r,θ,z	Cylindrical coordinate system	$[m]$
R_{ij}	Reynolds stress tensor with $i,j=(r,\theta,z)$	$[m^2/s^2]$
v'_r, v'_θ, v'_z	Fluctuating velocity components	$[m/s]$
V_r, V_θ, V_z	Mean velocity components	$[m/s]$

Non dimensional groups

C_p	Pressure coefficient	$\frac{P-P(r/b=0.92)}{0.5\rho\Omega^2 b^2}$
C_w	Voluminal flowrate coefficient	$Q/(\nu b)$
G	Aspect ratio of the cavity	h/b
Re	Rotational Reynolds number	$\Omega b^2/\nu$

Subscripts

$*$	normalized quantity
r	radial
θ	tangential
z	axial

Greeks

ε	Dissipation rate of the turbulence kinetic energy	$[m^2/s^3]$
ν	Kinematic viscosity of the fluid	$[m^2/s]$
ω	Specific dissipation rate	$[1/s]$
Ω	Rotation rate of the rotating disk	$[rad/s]$
Ψ	Stream function	$[-]$
ρ	Density	$[kg/m^3]$

INTRODUCTION

A proper modeling of the phenomena connected with turbulence improves the quality of CFD calculations of the flow through turbine stages and cavities since the investigations of heat transfer (7), skin friction (8), flow separation and reattachment effects strongly depend on the correct simulation of turbulence. In such a way, even if the CFD has been accepted as a design tool, the accurate prediction of main rotating cavity flows still remains a challenging task.

Chew (9) was the first to study the flow inside a rotor-stator cavity with centrifugal throughflow using a k-ε model. Chew and Vaughan (10) studied this type of flow with and without imposed throughflow with a model based on a mixing length hypothesis inside the whole cavity. Their results were quite comparable to the experimental data of Daily and Nece (11) and Daily et *al*. (12) apart from a relaminarization area close to the rotating axis. The model of Iacovides and Theofanopoulos (13) used two zonal approaches based on an algebraic modeling of the Reynolds stress tensor in the fully developed turbulence area and a mixing length hypothesis near the wall. They compared them to two k-ε models in both the corotating disk configuration and the rotor-stator problem with or without throughflow. The authors concluded that these approaches are cost-effective methods and that neither of these two zonal modelings appeared to be universally successful in these configurations. Iacovides and Toumpanakis (14) tested four turbulence models and showed that the Reynolds Stress Model (RSM) was an appropriate level of closure to describe rotor-stator flows in an enclosed cavity. Schiestel et *al*. (15) have used a k-ε model near the walls and an Algebraic Stress Model (ASM) in the core of the flow. Second-order information was found to be necessary in turbulence closure to get a sufficient degree of universality in predicting rapidly rotating flows.

Virr et *al*. (16) presented validation studies, based on turbine disk cavity flows, showing that CFD was a valuable design tool capable of predicting flow at engine operating conditions. The standard k-ε turbulence model with wall functions and a two layer k-ε/k-l model were used. Limitations of the wall function method were identified at low rotational Reynolds numbers. However, this method gave acceptable results at higher Reynolds numbers, more representative of engine conditions. The two layer model has shown greater generality. These conclusions were consistent with earlier studies, and have been confirmed by other authors, as shown in the CFD validation table presented by Smout et *al*. (17). In their review of the flow in rotating systems with radial outflow, Wilson et *al*. (18) showed also that the flow and heat transfer in such systems can be computed with acceptable accuracy using k-ε models.

Elena and Schiestel (3) proposed some numerical calculations of rotating flows with and without throughflow. They compared three different turbulence models: a k-ε low Reynolds number model, a zonal modeling using a RSM linked to a k-ε model near the walls and a fully Reynolds stress transport closure (RSM) derived from the Launder and Tselepidakis (19) one. Elena and Schiestel (4) modified this previous version of the RSM model to take into account the implicit effects of rotation on turbulence. These authors (3; 4) pointed out that the RSM model is the adequate level of closure compared to the classical k-ε model or to the ASM approach to describe turbulent rotating disk flows with or without an imposed in- or outflow. Iacovides et *al*. (20) tested two low Reynolds number turbulence models: a classical k-ε model and a modified RSM, which takes into account rotation effects. More recently, Poncet et *al*. (1; 2) compared pressure and velocities measurements to numerical predictions based on an improved version of the RSM of Elena and Schiestel (4). All the comparisons were in excellent agreement for the mean and turbulent fields in all operating conditions including rotor-stator in an enclosed cavity or with an inward or outward throughflow. Very recently, Craft et *al*. (21) examined the swirling flow inside an enclosed rotor-stator cavity within a RANS framework. They developed a three-dimensional and unsteady low Reynolds number k-ε model. Some computations revealed large-scale vortical unsteady structures embedded in the core region between the disks, structures very similar to the ones observed experimentally by dye injection.

Some authors use alternative models, such as the k-ω SST model of Menter (22). Jarzombek et *al*. (23) applied it to a pre-swirl chamber, and it appears that, with care, a number of the commonly available eddy viscosity models may be used for disk cavity flows. Other authors focused their investigations on the application of standard turbulence models in solving swirled flow in rotating cavities (24; 25; 26). Wu et *al*. (24) presented a CFD benchmark of the flow within rotor-stator, contra-rotating and co-rotating disk cavities. The authors tested several turbulence models and the k-ω SST model offered the best agreement with the experimental data. Debuchy et *al*. (25) focused their works on the comparison of CFD predictions obtained with a two equation k-ω SST turbulence model with experimental measurements carried out by hot-wire anemometry and three-holes pressure probes. The authors reveal that the experiments are well described qualitatively by numerical results. Roy et *al*. (26) performed axisymmetric CFD analyses by simulating the turbulence in a shrouded rotor-stator cavity. In comparison with measured velocity profiles, the k-ω SST model demonstrated the best overall agreement. The reader can refer to the review of Owen and Wilson (27) for recent computational research on rotating disk flows including rotor-stator systems with throughflow.

Bearing in mind the mentioned contributions, emerges that the selection of a suitable turbulence model for the study of rotor-stator cavity flows, remains an open issue in the literature. That is the reason why a numerical assesment of turbulence model in

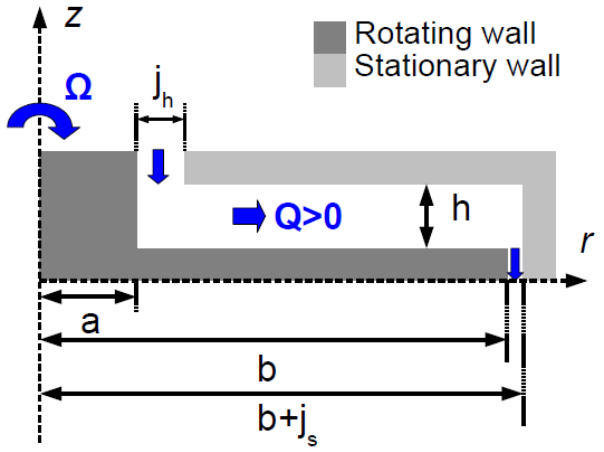

Figure 1. Schematic representation of the experimental set-up and notations. $a + j_h = 55$ mm is the radius of the central opening, $a = 38$ mm and $b = 250$ mm the inner and outer radii of the rotating disk and $b + j_s = 253$ mm the outer radius of the cavity whose height h is here fixed to 9 mm.

a gas turbine rotor-stator system is proposed in the present work. Generally speaking, second order turbulence modeling could provide a better prediction of the turbulence field with respect to the eddy viscosity based models. On the other hand, traditional two equation turbulence models are widely used in the industry due to both their numerical stability and the favourable impact on the calculation cost. The aim of the present contribution is to point out if the traditional two equation turbulence models could be assumed as reliable instruments for the prediction of the fluid flow within rotor-stator systems. Several standard two equation models were considered in their native form implemented within the CFD code CFX-12.0. The analysis was conducted on an experimental rotor-stator shrouded cavity implemented on a test rig at the IRPHE's laboratory in Marseilles (1; 2; 28). The obtained results were also compared with those previously obtained by Poncet et *al*. (1; 2) by the use of a Reynolds Stress Modeling sensitized to rotation effects by Elena and Schiestel (4). Several configurations, covering a wide range of real engine operating conditions, were considered covering inflow, outflow and no superimposed flow cases. The paper is then organized as follows: the experimental setup and the turbulence modeling are described in the following sections. Then, the comparisons between the different approaches are proposed for the closed cavity case and then, when a centrifugal then centripetal throughflow is enforced. Some concluding remarks and future views are finally provided.

EXPERIMENTAL SETUP

Extensive velocity and pressure measurements have been performed using the test rig facility of the IRPHE's laboratory in Marseilles by the means of a Laser Doppler Anemometer (LDA) and pressure transducers.

Apparatus

The cavity sketched in figure 1 is composed of two smooth parallel disks: a fixed disk (the stator) facing a rotating one (the rotor) and separated by an axial gap $h = 9$ *mm*. A fixed shroud encloses the cavity. The rotor and the central hub attached to it rotate at the uniform angular velocity Ω by the means of a 5.5 kW electric servomotor. A pump allows to impose a variable voluminal throughflow Q, which can be either centrifugal ($Q > 0$) or centripetal ($Q < 0$).

The mean flow is mainly governed by three control parameters: the aspect ratio G of the cavity, the Reynolds number Re based on the outer radius b of the rotor, and the flowrate coefficient C_w, defined as follows:

$$G = \frac{h}{b} \qquad Re = \frac{\Omega b^2}{\nu} \qquad C_w = \frac{Q}{\nu b}$$

where ν is the kinematic viscosity of water. Note that the aspect ratio is fixed to $G = 0.036$ for all calculations.

The accuracy on the measurement of the angular velocity and on the flux is better than 1%. The cavity is maintained at rest at a pressure of 2 bar using a tankbuffer. The temperature is also maintained constant (296 K) using a heat exchanger, which allows to remove the heat produced by friction in order to keep constant the properties of water.

Measurement Techniques

The measurements were performed at the IRPHE's laboratory in Marseilles by means of a two-component LDA system and by pressure transducers. The LDA technique is used to measure, from above the fixed disk, the mean radial $V_r^* = V_r/(\Omega r)$ and tangential $V_\theta^* = V_\theta/(\Omega r)$ velocity components as well as the three Reynolds stress tensor components $R_{rr}^* = \overline{v_r'^2}/(\Omega r)^2$, $R_{r\theta}^* = \overline{v_r' v_\theta'}/(\Omega r)^2$, $R_{\theta\theta}^* = \overline{v_\theta'^2}/(\Omega r)^2$ in a vertical plane (r,z) at a given azimuthal angle. v_r' and v_θ' are the fluctuating parts of the radial and tangential velocity components and r is the radial location. The LDA method is based on the accurate measurement of the Doppler shift of laser light (error margin of $\pm 3\%$ on the mean velocities and $\pm 5\%$ on the second-order momentums) scattered by particles, 30 μm in diameter, carried with the fluid. It has been verified that 5000 validated data are sufficient to obtain the statistical convergence of the measurements. Note that the size of the probe volume (0.8 mm in the axial direction) is not negligible compared to the boundary layer thicknesses δ: for example $\delta \simeq 2.5\sqrt{\nu/\Omega} \simeq 0.6$ mm at $Re = 10^6$.

Pressure is measured by six accurate piezoresistive transducers (0.05% in the range 10-40 $^\circ C$), combining pressure sensors and temperature electronic compensations. Nevertheless, according to the experimental conditions, the accuracy on the pressure is about 5%. One direct consequence of the Taylor-Proudman theorem, which forbids axial gradients in rapidly rotating flows, is that the pressure on both disks are identical at the same radius within 2.5% accuracy. Thus, the transducers have been fixed on the stator at the following radial locations 0.093, 0.11, 0.14, 0.17, 0.2, and 0.23 m disposed along two rows because of experimental constraints. The reader can refer to the previous works of Poncet et *al*. (1; 28) for more details about the experimental setup.

NUMERICAL MODELING

In the next section, a brief description of the turbulence models used in this work is given. Finally the RSM model previously used by Poncet et *al*. (1; 2) is presented.

Turbulence Modeling using CFX-12.0

Two Equation Turbulence Models The standard k-ε and k-ω SST models in their formulation kept available by the commercial CFD 3D solver CFX-12.0 have been selected for all calculations presented here. Further more some tests were conduced using the innovative k-ω SST-CC proposed by Smirnov and Menter (5) and the k-ω SST-RM that takes in to account the reattachment modification proposed by Menter (6). All models were used in their original form, i.e. no tuning of the turbulence model constants was done.

k-ε model

The k-ε turbulence model solves two transport equations, one for the turbulence kinetic energy k and the other one for its dissipation rate ε. As usual for the two equation model, the transport equation for k is derived from the exact equation, while the equation for its dissipation rate is obtained using physical reasoning. In its original form and in its formulation kept available in CFX-12.0, the k-ε model is not sensitized to rotation and curvature effects. Accordingly with the CFD code restrictions (29), wall functions are used to evaluate the turbulence kinetic energy and its dissipation rate near solid walls.

k-ω SST model

The k-ω SST turbulence model solves two transport equations, one for the turbulence kinetic energy k and one for the specific dissipation ω. The idea of the SST model is to retain the robust and accurate formulation of the Wilcox k-ω model in the near wall region (22), and to take advantage of the free stream independence of the k-ε model in the outer part of the boundary layer. To achieve this, a k-ω formulation of a standard k-ε model is derived and merged together with the previous model via a blending function being one in the near wall region to activate the standard k-ω model and zero outside activating the k-ε model (29). In its standard formulation kept available by CFX-12.0, the k-ω SST is also not sensitized to flow rotation and curvature. Both low and high Reynolds approaches are used to evaluate the turbulence kinetic energy and its dissipation rate near solid walls.

k-ω SST-CC model

Recently, Smirnov and Menter (5) have applied to the k-ω SST the modification proposed by Spalart and Shur (30), to sensitize the two equation turbulence model to the rotation and curvature effects. The resulting k-ω SST Curvature Correction (CC) was deeply tested and the results of these validation studies are available in the literature (5). Basically, the model correction results in a multiplicative factor of the transport equation production term. This factor is expressed as complex function of the stress tensor S and the vorticity tensor Ω_{vort}. For further details on the correction term and in its implementation in CFX-12.0, the reader can refer to the work of Smirnov and Menter (5). A low Reynolds approach is used in the present work to evaluate the turbulence kinetic energy and its dissipation rate near solid walls.

k-ω SST-RM model

Most of the RANS models can predict the separation point accurately. Despite that, it is a well know deficiency in all k-ω models that the reattachment location is often predicted too far downstream to what is observed in experiments. So that a modification to the k-ω SST model has been developed by Menter and co-workers which improves this behavior (6). The mentioned correction results in a additional source term in the turbulence kinetic energy transport equation:

$$P_{reattach} = P_k \cdot min\left[4max\left(0, \frac{min\left(S^2, \Omega_{vort}^2\right)}{0.09\omega^2} - 1.6\right), 1.5\right] \quad (1)$$

where P_k represents the typical turbulence kinetic energy transport equation production term. In the present work, the k-ω SST-RM model was used in conjunction with a low Reynolds approach for the near wall treatment.

In-house second order closure

The Reynolds Stress Modeling of Elena and Schiestel (4) The approach presented by Poncet et *al*. (1; 2) is based on one-point statistical modeling using a low Reynolds number second-order closure derived from the Launder and Tselepidakis (19) model and sensitized to rotation effects by Elena and Schiestel (4). This approach allows for a detailed description of near-wall turbulence and is free from any eddy viscosity hypothesis. The general equation for the Reynolds stress tensor R_{ij} can be written as:

$$\frac{dR_{ij}}{dt} = P_{ij} + D_{ij} + \Phi_{ij} - \varepsilon_{ij} + T_{ij} \quad (2)$$

where P_{ij}, D_{ij}, Φ_{ij}, ε_{ij}, respectively, denote the classical production, diffusion, pressure-strain correlation and dissipation terms. The extra term T_{ij} accounts for the implicit effects of rotation on turbulence. Indeed, high-speed rotation produces indirect effects on the turbulence field that are not modeled in usual closures. These effects modify the structure of the turbulence eddies in a complex manner that can be evidenced in two-point statistics (31). A practical extension for one-point closures has been developed by Elena and Schiestel (4). It consists of additional terms in the stress transport equations that act only when the flow is subjected to strong rotation. More precisely, T_{ij} can be decomposed into four terms as follows:

$$T_{ij} = \Phi_{ij}^{(R)} + D_{ij}^{R} + B_{ij} + J_{ij} \quad (3)$$

where $\Phi_{ij}^{(R)}$ is a part of the pressure-strain correlation term sensitized to the dimensionality tensor C_{ij}. The modeling of its linear effect is deduced from the spectral tensor modeling of Schiestel and Elena (32). D_{ij}^{R} is an inhomogeneous diffusion term,

which slows down the tendency to bidimensionalization for wall bounded flows. B_{ij} is a homogeneous source term, which rectifies the pressure-strain correlation Φ_{ij} and which acts only in case of strong rotation. It produces spectral phase scrambling (angular dispersion). The rotation also reduces the energy transfer from large to small turbulent scales. It is modeled through an inverse flux J_{ij} considered as isotropic for high Reynolds number. It is a correction term of ε_{ij}, which increases the turbulence levels in the core of the flow. These four terms are defined as follows:

$$\Phi_{ij}^{(R)} = -0.6[(\mathcal{D}_{cij} + \frac{1}{2}\mathcal{D}_{c\Omega ij}) - \frac{2}{3}P_c\delta_{ij}] - \frac{2}{5}k(V_{i,j} + V_{j,i}) \quad (4)$$

$$D_{ij}^{R} = (c_s\frac{k^2}{\varepsilon}f_{Ro}Y_{lm}R_{ij,l})_{,m} \quad (5)$$

$$B_{ij} = -\alpha_B(R_{ij} - k\delta_{ij} + \frac{1}{2}C_{ij}) \quad (6)$$

$$J_{ij} = \frac{2}{3}[(1-f_T)\delta_{ij} + f_T\frac{3R_{ij}}{2k}]J \quad (7)$$

The dissipation rate equation ε is the one proposed by Launder and Tselepidakis (19). The turbulence kinetic energy equation, though it is redundant in a RSM model, is solved numerically in order to get faster convergence. The complete model is given in (4).

Numerical methods and computational details

CFD Solver Setup in CFX 12.0 and Numerical Grids

The fluid thermal and transport properties such as specific heat capacity, thermal conductivity and molecular viscosity, were kept constant. Energy equation was solved in terms of total energy including viscous heating effects. The convective fluxes were solved using a high order resolution scheme. As there is no evidence of three-dimensional structures embedded in the turbulent flow, the numerical domains consist in a 5° sector. All calculations presented here, are steady state adiabatic solutions. A mesh independence analysis was done. A 300×140 mesh in the (r,z) frame (y^+ values below 1) has proved to be sufficient for the low Reynolds calculations while a 240×70 mesh in the (r,z) frame (y^+ values from 30 to 150) was selected for the high Reynolds one. Some views of these two meshes are provided in figure 2. All meshes conunt 1 element in the tangential direction.

The numerical boundary conditions were imposed coherentely with the experimental setup. Mass flow rate and total temperature were prescribed at the domain inlet while static pressure was imposed at the outlet. In the case of an inward superimposed mass flowrate, the co-rotation factor is imposed equal to 0.5 at the cavity inlet. The convergence of the numerical simulations were primarily assessed by monitoring residuals of mass, energy and momentum equations. The required RMS residuals order of magnitude was below 10^{-7}. Furthermore, the runs were stopped when the physical quantities such temperature, pressure and velocity monitored in some monitor points have reached a steady state.

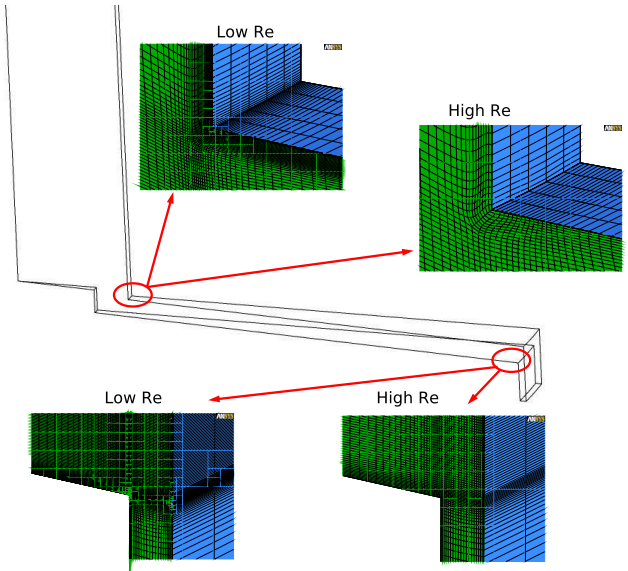

Figure 2. Calculation domain for the CFD computations using CFX 12.0 with some focus on the refined parts of the meshes for the low- and high-Reynolds number approaches.

Numerical method and computational details for the RSM The computational procedure is based on a finite volume method using staggered grids for mean velocity components with axisymmetry hypothesis in the mean. The computer code is steady elliptic and the numerical solution proceeds iteratively. A 140×80 mesh in the (r,z) frame proved to be sufficient in most of the cases to get grid-independent solutions. However, a more refined modeling 200×100 is necessary for the highest rotation rate corresponding to $Re = 4.15 \times 10^6$. Typically, the size of the first mesh in the axial direction is equal to $1.529 \times 10^{-4}h$ for the 140×80 mesh. In that case, the wall coordinate z^+ remains below 0.2 along both disks, which ensures an accurate description of the viscous sublayers. About 20000 iterations are necessary to obtain the numerical convergence of the calculation.

At the openings, V_θ is supposed to vary linearly from zero on the stationary wall up to Ωr on the rotating wall. When a throughflow is enforced, a parabolic profile is imposed for the axial velocity V_z at the inlet, with a given low level of turbulence intensity. In the outflow section, the pressure is fixed, whereas the derivatives for all the other independent quantities are set to zero if the fluids leaves the cavity, and fixed external values are imposed if the fluid re-enters the cavity. In the turbulent regime, the flow in the similarity area is practically not sensitive to the shape of profiles of tangential and axial velocity components or to the intensity level imposed at the inlet. By multiplying by a factor 3 the turbulence intensity level imposed at the inlet, the change is about 0.08% on the maximum of the turbulence kinetic energy in the whole cavity. Moreover, these choices are justified by the wish to have a model as universal as possible.

RESULTS

The rotor-stator configurations considered by Poncet et *al*. (1; 2) have been chosen for the present numerical benchmark. It includes enclosed and partially-open rotor-stator cavities with axial inward or outward throughflows. The different RANS mod-

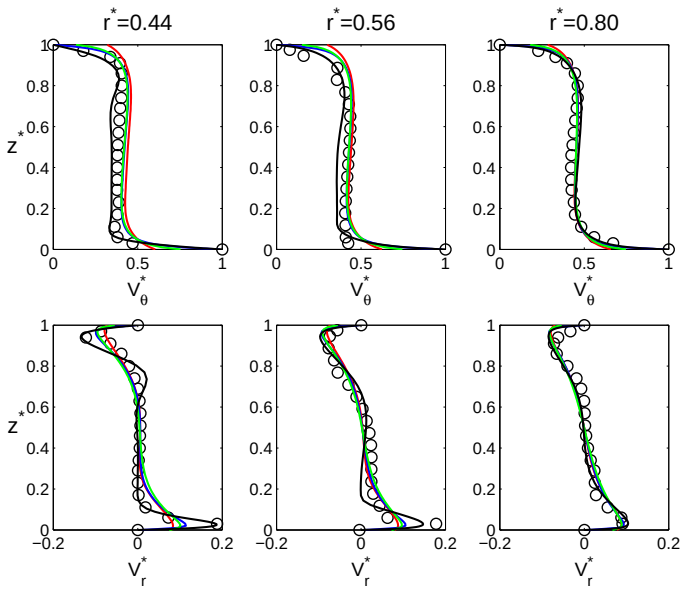

Figure 3. Axial profiles of the mean tangential and radial velocity components for $G = 0.036$, $Re = 1.038 \times 10^6$, $C_w = 0$ and three radial positions. Comparisons between the LDA measurements (○), the k-ε high Re (red lines), the k-ω SST low Re (blue lines), the k-ω SST high Re (green lines) and the RSM (black lines).

elings included in the CFD solver Ansys CFX 12.0 are compared to the RSM of Elena and Schiestel (4) and to the measurements of Poncet et *al*. (1; 2) in terms of velocities, turbulence intensities and pressure distributions.

Enclosed cavity

In this section, the base flow in an enclosed cavity without throughflow ($C_w = 0$) is considered. The aspect ratio of the cavity is fixed to $G = 0.036$, which corresponds to an intermediate gap ratio (11): $0.0179 \leq G \leq 0.0714$. According to these authors, the flow is laminar with merged boundary layers (regime I) up to $Re \simeq 4300$. As the rotation rate or the Reynolds number increases, the boundary layer thicknesses, which behave like $\sqrt{\nu/\Omega}$, get thinner and the flow becomes laminar with separated boundary layers (regime II). For $Re \geq 132000$, the flow is turbulent with merged boundary layers (regime III). When one increases further Re up to 389000, the flow remains turbulent but the boundary layers are separated (regime IV).

Figure 3 shows the axial profiles for the mean tangential and radial velocity components for $Re = 1.038 \times 10^6$ at three radial positions. The main flow is tangential due to the rotation of the lower disk. The aspect ratio G is large enough to ensure that the secondary flow in a (r,z) plane can be described by the Batchelor flow model: a centrifugal boundary layer on the rotor, called the Ekman layer, and a centripetal one on the stator, known as the Bödewadt layer, separated by a central inviscid core. In that region, the fluid rotates at some fraction of the rotor angular velocity and the radial velocity component is close to zero. Figure 4 shows typical streamlines for a cross section of a rotor-stator wheelspace: the fluid is pumped radially outwards along the rotor because of centrifugal effects moving axially across to the stator

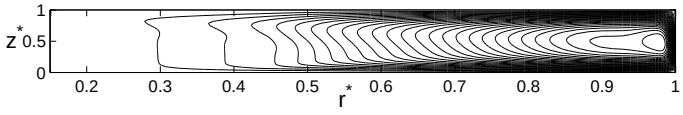

Figure 4. 26 streamline patterns obtained by the RSM for $G = 0.036$, $Re = 1.038 \times 10^6$ and $C_w = 0$ (apparent aspect ratio equal to 10).

in the boundary layer over the cylindrical outer shroud, known as the Stewartson layer. The fluid returns radially inward along the stator to come back close to the rotation axis and impinges on the hub. Then it is deflected axially to come back along the rotor. Thus, the mean axial velocity, which is not shown here, is quasi zero apart from the two regions along the inner and outer cylinders.

One interesting quantity in such flow is the value of the mean tangential velocity in the inviscid core called the swirl ratio and denoted β. It can be indeed directly linked to the radial pressure gradient through the cavity:

$$\frac{dP^*}{dr^*} = 2\beta^2 r^* \tag{8}$$

Equation (8) is the Navier-Stokes equation for the core region reduced using the evidence that $V_r^* \simeq V_z^* \simeq 0$ and $V_\theta^* = \beta$ in that core. The coefficient β has been the subject of an intense interest for many years (1; 12; 25; 28) because it permits to deduce the axial thrusts applied to the walls. Daily et *al*. (12) proposed the following correlation for the turbulent regime in a closed cavity: $\beta = 0.49 - 0.57G$. Thus, in the present case, $\beta = 0.47$, value slightly higher than the analytical one $\beta = 0.438$ proposed by Poncet et *al*. (28) and close to the measured one $\beta = 0.48$ by Daily and Nece (11). The values for β obtained by the different models are summarized in table 1. The high Reynolds modelings provide almost constant values along a radius, whereas the low-Reynolds modelings show an increase of β with r^*. The RSM predicts $\beta = 0.346$ at $r^* = 0.44$, which is characteristic of the laminar regime (33). The other models overestimate β at the first radial position. At the outer location, the RSM provides $\beta = 0.47$ in agreement with Daily et *al*. (12), while the other models predict a swirl ratio of 0.45, slightly higher than the experimental value. To sum up, the results of the RSM reveal a transitional flow within the cavity with a laminar behavior close to the hub and a turbulent regime at the periphery, whereas all the other models predict a turbulent flow at all radii. At $r^* = 0.44$, the local Reynolds number $Re_r = r^{*2} Re$ is equal to 2.01×10^5. For this value, the experiments of Itoh et *al*. (34) revealed that the flow is transitional with a turbulent boundary layer along the stator and a laminar boundary layer along the rotor, in agreement with Daily and Nece (11). Itoh et *al*. (34) found indeed that the Ekman layer becomes turbulent for $Re_r = 3.6 \times 10^5$.

From a general point of view, the k-ε and k-ω SST models catch the value of the swirl ratio as well as the mean velocity profiles. As it can be seen from figure 3, the RSM significantly improves the prediction of the mean velocity profiles in the very thin boundary layers. The boundary layer thicknesses but also

β	$r^* = 0.44$	$r^* = 0.56$	$r^* = 0.80$
LDA data	0.381	0.432	0.428
k-ε high Re	0.442	0.443	0.454
k-ω SST high Re	0.42	0.429	0.452
k-ω SST low Re	0.423	0.431	0.454
RSM low Re	0.346	0.365	0.47

Table 1. Values of the swirl ratio β for three radial locations and $G = 0.036$, $Re = 1.038 \times 10^6$, $C_w = 0$. Comparisons between the different approaches.

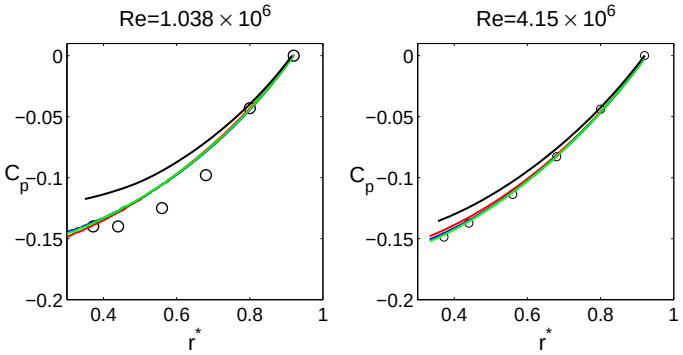

Figure 5. Radial pressure distributions for $G = 0.036$, $C_w = 0$ and two Reynolds numbers. Comparisons between the pressure measurements (○), the k-ε high Re (red lines), the k-ω SST low Re (blue lines), the k-ω SST high Re (green lines) and the RSM (black lines).

the extrema of the radial velocity are well captured.

To complete the comparisons for the mean field, pressure measurements have been performed by means of six pressure transducers located on the stator along two rows because of geometrical constraints. We choose to take as a reference the pressure measured at the outer radial position $r^* = 0.92$ to define the pressure coefficient: $C_p(r^*) = P^*(r^*) - P^*(r^* = 0.92)$. The dimensionless pressure is given by: $P^* = P/(0.5\rho\Omega^2 b^2)$, where ρ is the density of water. In figure 5, is plotted the pressure coefficient versus the dimensionless radial position for two values of the Reynolds number. As expected, the pressure decreases towards the center of the cavity: C_p is then always negative. Note that the values in these cases are relatively weak. The RSM model slightly underestimates the values of C_p (in absolute value) close to the rotation axis, which is directly linked to the underestimation of the swirl ratio β (shown at $r^* = 0.44$ in figure 3 for $Re = 1.038 \times 10^6$) through the equation (8). Between $Re = 1.038 \times 10^6$ and $Re = 4.15 \times 10^6$, there is no evident effect of the Reynolds number on the pressure distribution. The maximum value of $|C_p|$ at $r^* = 0.372$ is equal to 0.15 in both cases.

Concerning the turbulent field, the Reynolds stresses are directly computed in the RSM modeling through the equation (2). To evaluate the Reynolds stresses using the models contained in CFX 12.0, we used the following formula:

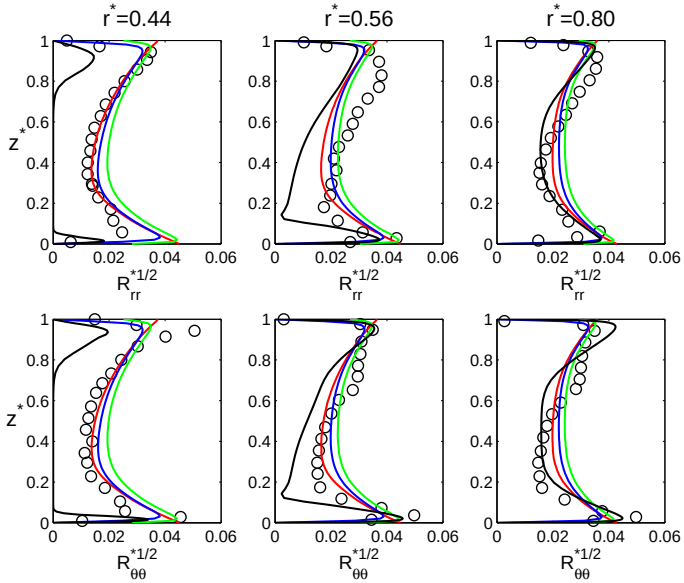

Figure 6. Axial profiles of two normal components of the Reynolds stress tensor. See legend of Figure 3.

$$R_{ij} = \frac{2}{3}k\delta_{ij} - \nu_T(V_{i,j} + V_{j,i}) \tag{9}$$

with $\nu_T = c_\mu k^2/\varepsilon$ ($c_\mu = 0.09$) for the k-ε model and $\nu_T = k/\omega$ for the k-ω models. The numerical results are compared to the experimental data for two normal components of the Reynolds stress tensor measured by the LDA system. The axial profiles for the two normal components R^*_{rr} and $R^*_{\theta\theta}$ are presented at three radial locations in figure 6. The boundary layers are turbulent whereas the core remains laminar. Turbulence intensities increase when moving towards the periphery, which is an effect of an increase in local Reynolds number. It is not so clear from figure 6 as the Reynolds stresses are normalized by the local disk velocity. The results obtained by CFX 12.0 do not show any radial dependence of the profiles, while the results obtained using the RSM confirm the transition from a laminar behavior at $r^* = 0.44$ ($Re_r = 2.01 \times 10^5$) to a turbulent regime at $r^* = 0.8$ ($Re_r = 6.64 \times 10^5$). Thus, for $r^* \leq 0.56$, where the flow is transitional, the RSM underpredicts the right profiles. At the outer radius $r^* = 0.8$, a better overall agreement is obtained using the RSM. The two equation models provide similar and quite satisfying results in that case. Note that the cross component $R^*_{r\theta}$ is not shown here because the RANS models used have shown that it remains quite weak within the cavity in agreement with the experiment (1).

Outward throughflow

The effect of an outward throughflow on the base flow previously described is here investigated for $G = 0.036$, $Re = 1.038 \times 10^6$ and $C_w = 5159$. We recall that the incoming fluid enters the cavity axially and leaves it axially also as shown from

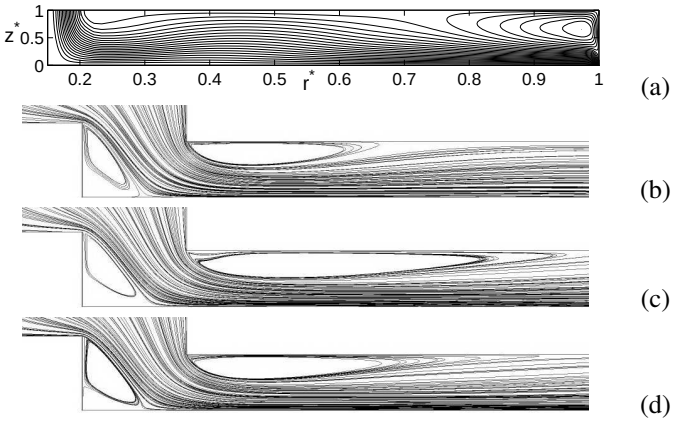

Figure 7. Streamline patterns obtained by (a) the RSM (apparent aspect ratio equal to 10), (b) the k-ε high Re, (c) the k-ω SST low Re and (d) the k-ω SST low Re with the reattachement modification for r^* up to 0.661. Results obtained for $G = 0.036$, $Re = 1.038 \times 10^6$ and $C_w = 5159$.

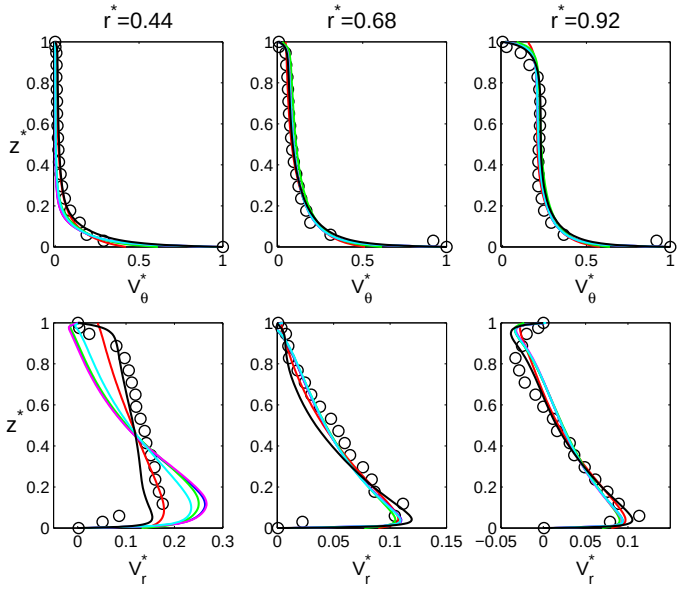

Figure 8. Axial profiles of the mean tangential and radial velocity components for $G = 0.036$, $Re = 1.038 \times 10^6$, $C_w = 5159$ and three radial positions. Comparisons between the LDA measurements (○), the k-ε high Re (red lines), the k-ω SST low Re (blue lines), the k-ω SST high Re (green lines), the k-ω SST-CC low Re (magenta lines), the k-ω SST-RM low Re (cyan lines) and the RSM (black lines).

the streamline patterns in figure 7a. Apart very close to the rotation axis where the flow impinges on the rotating disk, the flow is purely centrifugal in the main part of the cavity. From $r^* = 0.76$ to the shroud, a large recirculation bubble appears along the stationary disk. In that region, the flow is centripetal along the stator and centrifugal along the rotor exhibiting a Batchelor-like flow structure. Note that, even if the flow is open to the external environment, the radial gap between the rotor and the shroud j_s is small enough ($j_s/b = 0.012$) to prevent the ingestion of fluid coming from the external surroundings.

The mean velocity profiles are exhibited in figure 8 at three radial locations. When a superimposed supply of fluid is provided, the flow structure in the rotor-stator cavity is altered. Close to the hub at $r^* = 0.44$, the mean flow is well described by the Stewartson model (35): the tangential velocity in the rotor boundary layer reduces from the rotor speed value to zero away from the boundary layer with no core rotation, as in the free disk flow. Moving towards the periphery of the cavity, the swirl ratio, which is equal to 0 at $r^* = 0.44$, increases and the flow structure switches progressively to the Batchelor model (36) at $r^* = 0.92$. All models catch the transition between these two flow structures regarding the mean tangential velocity profiles.

The radial superimposed throughflow is large enough in the present case ($C_w = 5159$) to suppress the inward flow observed along the stator in the closed cavity case. Thus, the mean radial flow is purely centrifugal at $r^* = 0.44$ (see also figure 7a) with a maximum in the Ekman layer because of the joint effects of the centrifugal force and the imposed throughflow. At the outer radial location $r^* = 0.92$, the flow is of Batchelor type and the outward flow is not sufficient to suppress the inward flow in the Bödewadt layer. Even if all models provide similar results for $r^* = 0.68$ and $r^* = 0.92$, the RSM slightly improves the predictions in the boundary layers. At $r^* = 0.44$, only the RSM and more surprisingly the k-ε high Reynolds approach offer a good agreement against the experimental data for the radial velocity component. All the other RANS models fail to predict the right profiles with a large overestimation of the outward flow along the rotor and by conservation of mass, an underestimation of the outward flow along the stator. It can be explained by looking at the streamline patterns exhibited in figure 7. Close to the cavity entrance, a separation zone due to the stator sharp edge, is predicted by all calculations presented here. The separation bubble dimension is strongly related to the flow turbulence kinetic energy. As remarked by Bradshaw (37), concave streamline curvature leads to an increase of turbulence kinetic energy. Following that way, the overestimation of the separation bubble dimension predicted by the k-ω models could be addressed to a poor prediction of the flow curvature effects on turbulence. On the other hand, the well known separated flow turbulence kinetic overestimation done by the k-ε model leads, in the present case, to a better prediction of the separated zone extension.

Even if the reattachment modification limits the separation bubble extension (figure 7d), the radial velocity profile prediction is not improved significantly by the use of the k-ω SST-RM turbulence model as shown in figure 8. The curvature correction implemented within the k-ω SST-CC model, seems to provide similar results to those obtained by the use of the standard k-ω SST (figure 8).

The radial distribution of the pressure coefficient C_p is displayed in figure 9. The maximum values reached by $|C_p|$ are quite comparable to the closed cavity case. A strong increase in $|C_p|$ is observed close to the rotation axis because of the impinging jet. All models provide the good trend but the RSM matches quite well with the pressure measurements.

The turbulent field is clearly affected by the outward throughflow comparing figures 3 and 8. It is noticeable that all models provide the same profiles for R^*_{rr} and $R^*_{\theta\theta}$ at these three radial locations. Turbulence intensities are mainly confined

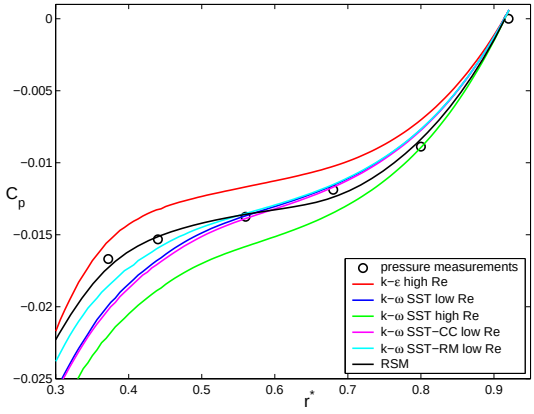

Figure 9. Radial pressure distributions. See legend of figure 8.

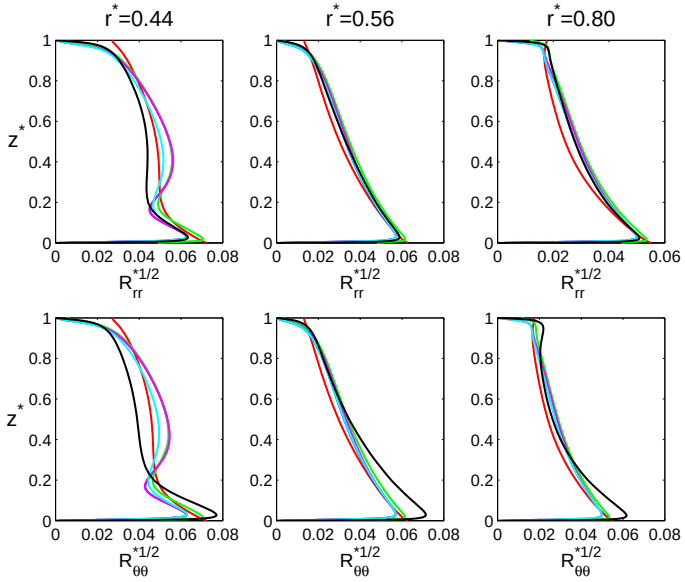

Figure 10. Axial profiles of two normal Reynolds stress tensor components. See legend of figure 8.

along the rotor and decrease continuously with z^* to vanish at the stator side. R_{rr} and $R_{\theta\theta}$ slightly increase when moving towards the periphery of the cavity because of an increase in local Reynolds number Re_r but due to the normalization by $(\Omega r)^2$, R^*_{rr} and $R^*_{\theta\theta}$ slightly decrease with r. As no experimental data are available for the turbulent field, no definitive conclusion can be drawn from these comparisons.

Inward throughflow

The fluid is now supplied inward to the space between the rotating and the stationary disk at a flowrate of $C_w = -5929$. The aspect ratio and the Reynolds number are kept constant: $G = 0.036$ and $Re = 1.038 \times 10^6$. From the streamlines displayed in figure 11, it can be seen that the flowrate coefficient is here large enough to suppress, in the main part of the cavity ($r^* \lesssim 0.56$), the outflow otherwise generated by disk pumping, which confirms the previous results of Bayley and Canary (38) for the

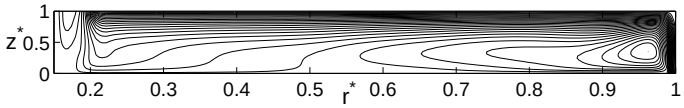

Figure 11. 26 streamline patterns obtained by the RSM for $G = 0.036$, $Re = 1.038 \times 10^6$ and $C_w = -5929$ (apparent aspect ratio equal to 10).

case of an open rotor-stator system with a net radial superposed inflow. At $r^* \simeq 0.56$, the presence of a point of radial stagnation is observed on the rotating disk (see also figure 12). Thus, the flow structure within the cavity can be decomposed into three regions as proposed by Pincombe (39) from flow visualizations:

1. at large radii ($r^* \geq 0.56$), the inflow has difficulty penetrating and a large recirculation bubble is observed along the rotating disk: it is the rotationally dominated regime.
2. at lower radii ($r^* \leq 0.56$), the flow is in the inflow dominated regime with a purely centripetal flow within the gap.
3. around the radial stagnation point ($r^* \simeq 0.56$), an intermediate regime is observed, where the flow combines both rotational and inflow effects.

The gap between the stator and the hub j_h is large enough ($j_h/b = 0.068$) to observe an ingestion of fluid coming from the external environment in the outflow region. These results are comparable to the qualitative representation of the pseudo-streamlines that Owen and Rogers (33) observed from their numerical simulations.

The effect of the centripetal throughflow on the mean velocity profiles is presented in figure 12. The tangential velocity in the core increases compared to the closed cavity case. The swirl ratio β reaches 1.56 at $r^* = 0.44$ and decreases to 0.74 at $r^* = 0.8$ by conservation of the angular momentum. The profiles at $r^* = 0.56$ confirm the presence of a point of radial stagnation around this location. Thus, $\beta \simeq 1$ at $r^* = 0.56$ and the mean radial velocity component is almost equal to 0 at the rotor side. At $r^* = 0.44$, the flow is in the inflow dominated regime with a negative radial velocity within the boundary layers. At higher radii, the inflow is reduced along the rotating disk due to the centrifugal force. At the outer radius, the profile of the mean tangential velocity component presents the properties of a Batchelor flow without flux. An outward flow is also observed along the rotor indicating that rotation effects are dominant.

The models contained in CFX 12.0 give similar results in good agreement with the experimental data for V^*_θ, while the RSM model underpredicts the swirl ratio in the whole cavity. The explanation is that the swirl ratio β within the cavity strongly depends on the swirl imposed at the inlet. The swirl of the incoming fluid is found in the experiments to increase with the flow rate coefficient from 0.5 for $C_w = 0$ to 0.56 for $C_w = -10317$. In the RSM model, we recall that we impose a linear profile for V^*_θ at the inlet. It varies from 0 on the shroud to 1 on the rotor. This choice is justified by the wish to have a code as universal as possible. A turbulent Batchelor profile imposed at the inlet with a swirl ratio calibrated using the experimental value should improve significantly the predictions of the RSM model.

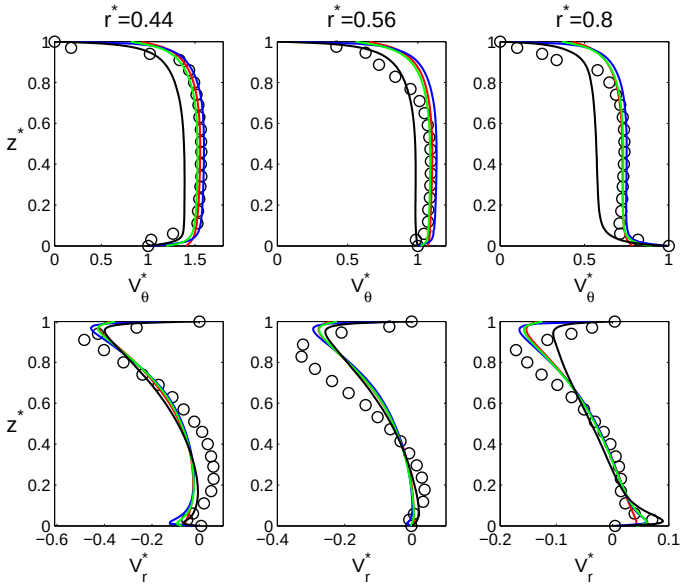

Figure 12. Axial profiles of the mean tangential and radial velocity components for $G = 0.036$, $Re = 1.038 \times 10^6$, $C_w = -5929$ and three radial positions. Comparisons between the LDA measurements (○), the k-ε high Re (red lines), the k-ω SST low Re (blue lines), the k-ω SST high Re (green lines) and the RSM (black lines).

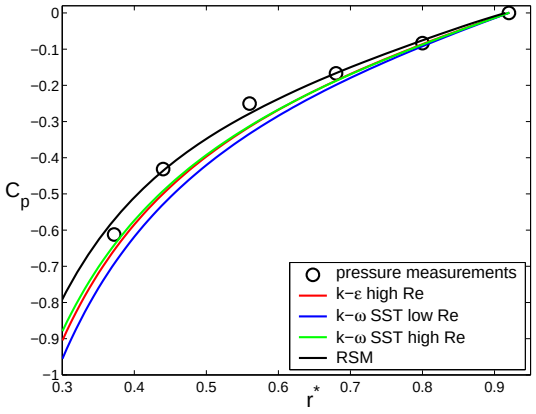

Figure 13. Radial pressure distributions for $G = 0.036$, $Re = 1.038 \times 10^6$ and $C_w = -5929$.

As shown in figure 13, the inflow induces a large pressure drop within the cavity: C_p approaches -0.8 for $r^* = 0.3$ regarding the RSM profile. This pressure drop is about 6 times larger than in the closed cavity or outflow cases. The RSM slightly improves the predictions of the radial pressure distribution compared to the other models.

Figure 12 shows the axial profiles of two components of the Reynolds stress tensor at three radial locations. The values of these normal components are quite comparable in the whole cavity. The Bödewadt layer along the stator is much more turbulent than the Ekman layer on the rotor. The flow appears to be more turbulent close to the axis of rotation than at the periphery of the cavity. The maximum values are much higher than in the closed

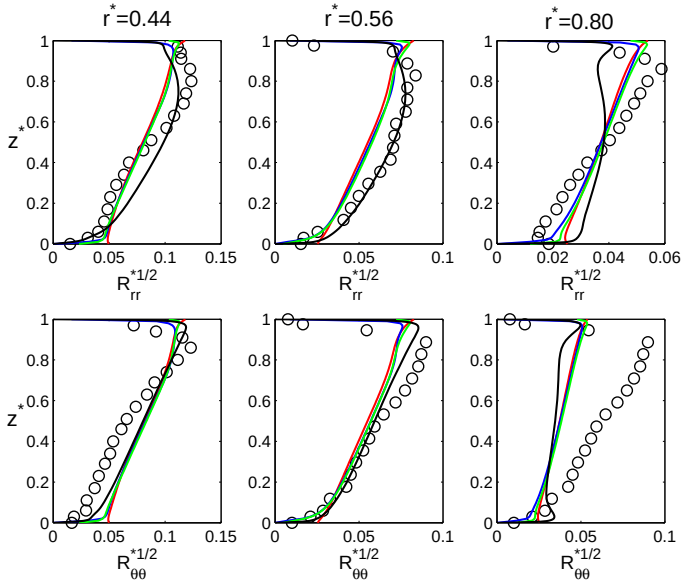

Figure 14. Axial profiles of two normal components of the Reynolds stress tensor. See legend of Figure 12.

cavity case and quite comparable to the outward flow one.

The RSM results are in good agreement with the experimental data. The turbulent intensities are well predicted apart from at the outer radial location where peripheral effects may occur. The other models provide similar results and fail to predict the right profiles at $r^* = 0.44$ and $r^* = 0.56$ with almost linear profiles for the two normal components. At the outer location $r^* = 0.8$, all models underpredict the turbulence intensities and especially the R^*_{rr} component. It can be explained by a too much lower turbulence level imposed at the inlet.

Concluding remarks

Turbulence modeling and measurements of the turbulent flow in a rotor-stator cavity is a great challenge especially when a throughflow is superimposed. In the present work, we have compared several two equation models available in the CFD code CFX 12.0 with the second order RSM model of Elena and Schiestel (4) and experimental data performed at IRPHE (1) for a fixed geometry ($G = 0.036$), two Reynolds numbers and several relevant flowrates including inward and outward throughflows.

For an enclosed cavity, the flow structure is well described by the Batchelor model with two boundary layers separated by a central inviscid core. The normalized tangential velocity in that core, known as the swirl ratio, is in the range between 0.34 and 0.47. Turbulence intensities are confined within the very thin boundary layers. When an outward throughflow is enforced, both Batchelor and Stewarston models can be observed depending on the radial location. At inner radii, where the flow is mainly dominated by the throughflow, there is only one boundary layer on the rotor and no core region, it is the so-called Stewartson model. Closer to the periphery, the flow belongs to the Batchelor regime, because of the dominating effect of rotation. Nevertheless, the swirl ratio remains smaller than in the closed cavity case. Turbulence intensities are essentially confined along the rotating disk

where both rotation and throughflow act. On the contrary, when the throughflow is inward, the flow can be still decomposed into three flow regions. At $r^* = 0.44$, the central core rotates faster than the disk and both boundary layers are centripetal: it is the inflow dominated regime. The presence of a stagnation point of zero radial velocity has been observed around $r^* = 0.56$. After this radius, the flow recovers the Batchelor flow structure with a centrifugal flux along the rotor and a core rotating slower than the disk. Turbulence intensities are found to be maximum along the stator and decrease towards the rotor.

The results of the two equation models are in good agreement with the experimental data for both the mean and turbulent fields and all the operating conditions considered in the present work. Moreover, they all offered a fast and robust convergence of the calculations. Rotor-stator flows are known to be very sensitive to the swirl and turbulence levels imposed for the incoming fluid. That is the reason why the present RSM model, which has not be sensitized to the inflow conditions, tends to underestimate the swirl ratio in the presence of an inward throughflow. The analysis points out that the RSM improves the predictions compared to the other models, regarding the boundary layers profiles and for the turbulent field. On the other hand, as we could expect since 8 transport equations are solved instead of 2 for the other approaches, the calculation time is much longer. For industrial applications, the k-ω SST model seems to offer a good compromise between accuracy and calculation cost.

References

[1] Poncet, S., Chauve, M. P., and Schiestel, R., 2005. "Batchelor versus Stewartson flow structures in a rotor-stator cavity with throughflow". *Phys. Fluids,* **17**(7).

[2] Poncet, S., Schiestel, R., and Chauve, M. P., 2005. "Centrifugal flow in a rotor-stator cavity". *J. Fluid Eng.,* **127**, pp. 787–794.

[3] Elena, L., and Schiestel, R., 1995. "Turbulence modeling of confined flow in rotating disk systems". *AIAA J.,* **33**(5), pp. 812–821.

[4] Elena, L., and Schiestel, R., 1996. "Turbulence modeling of rotating confined flows". *Int. J. Heat Fluid Flow,* **17**, pp. 283–289.

[5] Smirnov, P. E., and Menter, F. R., 2008. "Sensitization of the SST turbulence model to rotation and curvature by applying the Spalart-Shur correction term". *ASME paper*(GT2008-50480).

[6] "Ansys inc. unpublished documentation".

[7] Da Soghe, R., Andreini, A., and Facchini, B., 2009. "Turbine stator well CFD studies: Effects of coolant supply geometry on cavity sealing performance". *ASME Journal of Turbomachinery*(1100, Press in progress).

[8] Da Soghe, R., Innocenti, L., Micio, M., and Facchini, B., 2009. "Analysis of gas turbine rotating cavities by an one-dimensional model: Definition of a new discs friction coefficients correlation set". *ASME Journal of Turbomachinery*(1088, Press in progress).

[9] Chew, J. W., 1984. "Prediction of flow in rotating disc systems using the k-ε model". *ASME paper*(84-GT-229).

[10] Chew, J. W., and Vaughan, C. M., 1988. "Numerical predictions of flow induced by an enclosed rotating disk". *ASME paper*(88-GT-127).

[11] Daily, J. W., and Nece, R. E., 1960. "Chamber dimension effects on induced flow and frictional resistance of enclosed rotating disks". *ASME J. Basic Eng,* **82**, pp. 217–232.

[12] Daily, J. M., Ernst, W. D., and Asbedian, V. V., 1964. Enclosed rotating discs with superimposed throughflow. Tech. rep., Dept. of Civil Engineering, Lab MIT, Rep. No. 64.

[13] Iacovides, H., and Theofanopoulos, I. P., 1991. "Turbulence modeling of axisymmetric flow inside rotating cavities". *Int. J. Heat Fluid Flow,* **12**(1), pp. 2–11.

[14] Iacovides, H., and Toumpanakis, P., 1993. "Turbulence modeling of flow in axisymmetric rotor-stator systems". *5th Int. Symp. on Refined Flow Modeling and Turbulence Measurements, Presses de l'École Nationale des Ponts et Chaussées*.

[15] Schiestel, R., Elena, L., and Rezoug, T., 1993. "Numerical modeling of turbulent flow and heat transfer in rotating cavities". *Numer. Heat Transfer Part A,* **24**(1), pp. 45–65.

[16] Virr, G. P., Chew, J. W., and Coupland, J., 1994. "Application of computational fluid dynamics to turbine disc cavities". *ASME Journal of Turbomachinery,* **116**, pp. 701–708.

[17] Smout, P. D., Chew, J. W., and Childs, P. R. N., 2002. "Icas-gt: A european collaborative research programme on internal cooling air systems for gas turbines". *ASME paper*(GT-2002-30479).

[18] Wilson, M., Chen, J., and Owen, J. "Computation of flow and heat transfer in rotating-disc systems". *3rd Int. Conf. on Computers in Reciprocating Engines and Gas Turbines, Trans IMechE*, pp. 41–49.

[19] Launder, B. E., and Tselepidakis, D. P., 1994. "Application of a new second moment closure to turbulent channel flow rotating in orthogonal mode". *Int. J. Heat Fluid Flow,* **15**(1), pp. 2–10.

[20] Iacovides, H., Nikas, K. S., and Te, M. A. F., 1996. "Turbulent flow computations in rotating cavities using low-reynolds-number models". *ASME paper*(96-GT-159).

[21] Craft, T. J., Iacovides, H., Launder, B. E., and Zacharos, A., 2008. "Some swirling-flow challenges for turbulent CFD". *Flow, Turbulence and Combustion,* **80**(4), pp. 419–434.

[22] Menter, F. R., 1994. "Two-equation eddy viscosity turbulence models for engineering applications". *AIAA J.,* **32**, pp. 1598–1605.

[23] Jarzombek, K., Dohman, H. J., Benra, F. K., and Scheider, O., 2006. "Flow analysis in gas turbine pre-swirl cooling air systems variation of geometric parameters". *ASME paper*(GT2006-90445).

[24] Wu, C., Vaisman, B., McCusker, K., and Paolillo, R., 2006. "Prediction of heat transfer coefficient in rotating cavities with radial outflow". *ASME paper*(GT2006-91078).

[25] Debuchy, R., Gatta, S. D., D'Haudt, E., Bois, G., and Martelli, F., 2007. "Influence of external geometrical modifications on the flow behaviour of a rotor-stator system: numerical and experimental investigation". *Proc. of the Institution of Mechanical Engineers, Part A: J. Power Energ.,* **221**(6), pp. 857–864.

[26] Roy, R. P., Zhou, D. W., Ganesan, S., Wang, C. Z., Paolillo, R. E., and Johnson, B. V., 2007. "The flow field

and main gas ingestion in a rotor-stator cavity". *ASME paper*(GT2007-27671).
[27] Owen, J. M., and Wilson, M., 2006. "Some current research in rotating-disc systems". *Annals New York Academy of Sciences,* **934**, pp. 206–221.
[28] Poncet, S., Chauve, M. P., and Gal, P. L., 2005. "Turbulent rotating disk flow with inward throughflow". *J. Fluid Mech.,* **522**, pp. 253–262.
[29] "Ansys inc, 2009. cfx-12.0 user's guide".
[30] Spalart, P. R., and Shur, M. L., 1997. "On the sensitization of turbulence models to rotation and curvature". *Aerospace Science and Technology,* **1**(5), pp. 297–302.
[31] Cambon, C., and Jacquin, L., 1989. "Spectral approach to non-isotropic turbulence subjected to rotation". *J. Fluid Mech,* **202**, pp. 295–317.
[32] Schiestel, R., and Elena, L., 1997. "Modeling of anisotropic turbulence in rapid rotation". *Aerosp. Sci. Technol.,* **7**, pp. 441–451.
[33] Owen, J. M., and Rogers, R. H., 1989. *Flow and Heat Transfer in Rotating Disc Systems. Volume 1 - Rotor-Stator Systems*. John Wiley & Sons Inc., New-York.
[34] Itoh, M., Yamada, Y., Imao, S., and Gonda, M., 1992. "Experiments on turbulent flow due to an enclosed rotating disc". *Exp. Thermal Fluid Sci.,* **5**, pp. 359–368.
[35] Stewartson, K., 1953. "On the flow between two rotating coaxial disks". *Proc. Camb. Phil. Soc.,* **49**, pp. 333–341.
[36] Batchelor, G., 1951. "Note on a class of solutions of the Navier-Stokes equations representing steady rotationally-symmetric flow". *Quat. J. Mech. and Appl. Math.,* **4**(1), pp. 29–41.
[37] Bradshaw, P., 1973. Effects of streamline curvature on turbulent flow. Tech. rep., Imperial College of Science and Technology.
[38] Bayley, F. J., and Conway, L., 1964. "Fluid friction and leakage between a stationary and rotating disc". *J. Mech. Eng. Sci.,* **6**, pp. 164–172.
[39] Pincombe, J. R., 1973. Flow visualisation and velocity measurements in a rotor-stator system with a forced radial inflow. Tech. rep., Thermo-Fluid Mechanics Research Centre, Univ. of Sussex (UK), Technical Note 88/TFMRC/TN61.